Design of IIR Filters for Active Noise Control by Constrained Optimization

Florian Hilgemann, Johannes Fabry, Peter Jax
Institute of Communication Systems (IKS)
RWTH Aachen University, Germany
{hilgemann,fabry,jax}@iks.rwth-aachen.de

***Abstract*—In the rapidly growing hearables market, active noise control (ANC) is a feature that customers increasingly demand. In this contribution, we present a design procedure for time-invariant infinite impulse response (IIR) feedforward filters for ANC applications. The filter minimizes a perceptually motivated cost function and can be computed using a nonlinear optimization solver. The design procedure yields filters that realize a user-defined active attenuation in the presence of constraints regarding stability and filter magnitude response.**

We verify the presented approach through simulation and real-time measurements for several design examples. Furthermore, we relate the achieved performance to an upper bound and investigate the impact of the constraints on the resulting performance.

***Index Terms*—Active noise control, acoustic equalization, constrained optimization, nonlinear optimization**

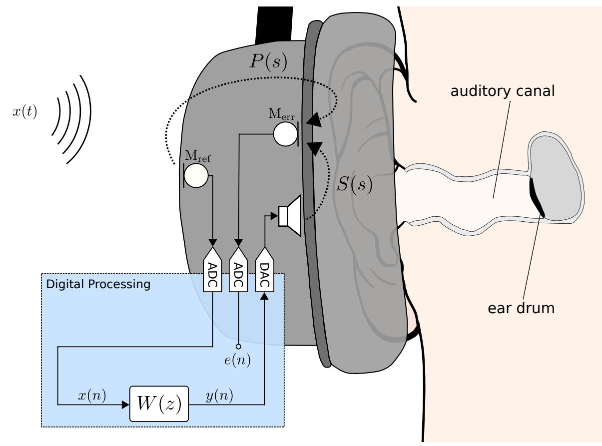

Fig. 1. Model of the digital AAE system (illustration not to scale).

I. Introduction

Exposure to noise has become increasingly common in today's society, causing a growing demand for insulation in hearable devices. In-ear and over-the-ear devices provide passive insulation, which tends to be insufficient at low frequencies. Active noise control (ANC) is able to complement passive attenuation favorably [1], [2].

Utilizing the capabilities of modern signal processors, ANC systems are typically implemented by means of digital filters. Since there is a direct connection between processing latency and performance, the filters are often operated at high sampling rates. Simultaneously, strict demands regarding algorithmic complexity and device form factor are imposed. Thus, pre-optimized time-invariant filters are often preferred to adaptive ones. Infinite impulse response (IIR) filters are especially well-suited for operation at high sampling rates since they require fewer resources than finite impulse response (FIR) filters. In addition, commercially available hardware platforms often only support second order sections (SOS).

Recently, active acoustic equalization (AAE) was proposed as a generalization to ANC which facilitates a fit to a user-defined overall magnitude response [3], [4]. Besides the well-known use-case ANC, it can also be employed to design an acoustically transparent ear-piece [5]–[7]. Despite the versatility it offers in terms of applications, AAE filter design methods have so far been limited to FIR filters. It is possible to convert the FIR filter to an IIR filter, however, this will likely impair the performance since the resulting filter is no longer optimal in terms of the original design criterion.

In this contribution, we investigate an approach to the design of IIR feedforward filters which is based on direct optimization. Intrinsically, this leads to a non-convex optimization problem. Thus, the solution depends on the starting point and is not guaranteed to be globally optimal [8]. However, we show that well performing solutions can be found by virtue of state of the art solvers for nonlinear optimization such as the sequential quadratic programming (SQP) algorithm. Another novelty is the explicit integration of constraints, which renders the presented approach flexible and versatile. We verify the approach by means of simulations and dummy head measurements.

II. System Overview

We consider a digital feedforward system as depicted in Figure 1, which we conceptually divide into an analog and a digital part. We denote analog signals with time t and systems with complex frequency s. In the digital domain, we denote signals with discrete time n and systems via complex frequency z. To ease notation we use the same names for continuous time and discrete time variables, e.g., $x(t) = x(nT)$, $P(s) = \mathscr{L}\{p(t)\}$ and $P(z) = \mathscr{Z}\{p(n)\}$ where $z = e^{sT}$.

The feedforward system utilizes an outward-facing microphone $\mathrm{M}_{\mathrm{ref}}$ with subsequent analog digital conversion to sense ambient sounds $x(t)$. The resulting digital signal $x(n)$ is filtered by a digital filter $W(z)$ to synthesize the digital control signal $y(n)$. By digital analog conversion with subsequent playback over the speaker, the system strives to realize a defined transfer function $H(s) = X(s)/E(s)$, i.e., a transfer function from the outward-facing microphone $\mathrm{M}_{\mathrm{ref}}$ to the inward-facing microphone $\mathrm{M}_{\mathrm{err}}$. An inward-facing microphone is needed only for calibration purposes, however, it is not required for operation of the system.

We characterize the analog system by acoustic transfer paths which are assumed to be time-invariant. Specifically, the transfer function from the outward-facing microphone $\mathrm{M}_{\mathrm{ref}}$ to the inner microphone $\mathrm{M}_{\mathrm{err}}$ is modeled via the primary path $P(s)$ and the transfer function from the loudspeaker to $\mathrm{M}_{\mathrm{err}}$ via the secondary path $S(s)$. We assume that acoustic feedback from the speaker to $\mathrm{M}_{\mathrm{ref}}$ is negligible because closed ANC headphones usually exhibit a good passive insulation.

III. Equalization Filter Design

We aim to design a digital cascade filter $W(z)$ which comprises L SOS such that a transfer function $H(s)$ from $\mathrm{M}_{\mathrm{ref}}$ to $\mathrm{M}_{\mathrm{err}}$ is realized. In other words, we are interested in obtaining a coefficient vector

$$\boldsymbol{\theta} = \begin{bmatrix} g & \boldsymbol{b}_1^{\mathrm{T}} & \boldsymbol{b}_2^{\mathrm{T}} & \boldsymbol{a}_1^{\mathrm{T}} & \boldsymbol{a}_2^{\mathrm{T}} \end{bmatrix}^{\mathrm{T}} \in \mathbb{R}^{4L+1} \tag{1}$$

which meets the defined design goal. In (1), g denotes a scaling factor, $\boldsymbol{b}_1$ and $\boldsymbol{b}_2$ each contain L numerator coefficients and $\boldsymbol{a}_1$ and $\boldsymbol{a}_2$ each contain L denominator coefficients. Using this notation, the filter response $W(\boldsymbol{\theta}, \Omega)$ becomes a function of $\boldsymbol{\theta}$ and the normalized frequency $\Omega \in [0, 2\pi)$, i.e.,

$$W(\boldsymbol{\theta}, \Omega) = g \cdot \prod_{l=1}^{L} \frac{1 + b_{1l} e^{-j\Omega} + b_{2l} e^{-2j\Omega}}{1 + a_{1l} e^{-j\Omega} + a_{2l} e^{-2j\Omega}}. \tag{2}$$

Given $W(\boldsymbol{\theta}, \Omega)$ and a pair of paths $P(\Omega)$ and $S(\Omega)$, we determine the achieved transfer path $\tilde{H}(\Omega)$ as

$$\tilde{H}(\Omega) = P(\Omega) - S(\Omega) W(\boldsymbol{\theta}, \Omega). \tag{3}$$

The optimization target is to minimize the distance between target response $H(\Omega)$ and achieved response $\tilde{H}(\Omega)$ where $\boldsymbol{\theta}$ is the optimization variable. We propose to minimize the squared logarithmic power spectral density (PSD) distance

$$\Delta\Phi_{\log}(\boldsymbol{\theta}, \Omega) = \Phi_{hh,\log}(\Omega) - \Phi_{\tilde{h}\tilde{h},\log}(\boldsymbol{\theta}, \Omega), \tag{4}$$

with

$$\Phi_{hh,\log}(\Omega) = 10 \log_{10} |H(\Omega)|^2 \tag{5a}$$

$$\Phi_{\tilde{h}\tilde{h},\log}(\boldsymbol{\theta}, \Omega) = 10 \log_{10} \left| \tilde{H}(\boldsymbol{\theta}, \Omega) \right|^2, \tag{5b}$$

which is related to the nonlinear loudness perception of the human ear [9]. Note that the phase response of $H(\Omega)$ is not considered in (4) because the human auditory system has a low sensitivity towards moderate phase response changes [10].

Since the time-invariant approach cannot adjust to runtime information, we utilize a training set $\mathcal{I}$ that reflects potential wearing situations. Therefore, we consider a training set $\mathcal{I}$ with I path pairs, which we distinguish using the path index $i = 1, 2, \ldots, I$. We assume that the paths in $\mathcal{I}$ represent the wearing situation accurately and without bias and strive for optimal average case performance [3], [4]. Consequently, we define a cost function $\mathcal{C}(\boldsymbol{\theta})$ as the mean squared logarithmic distance for I path pairs as

$$\mathcal{C}(\boldsymbol{\theta}) = \frac{1}{2\pi I} \sum_{i=1}^{I} \int_0^{2\pi} \Delta\Phi_{i,\log}^2(\boldsymbol{\theta}, \Omega)\, d\Omega \tag{6}$$

and refer to the *optimal* filter as global minimum of (6). For filters of suitable order, solving $\nabla_{\boldsymbol{\theta}} \mathcal{C}(\boldsymbol{\theta}) = \mathbf{0}$ for $\boldsymbol{\theta}$ is not a feasible approach as it leads to intricate terms. Instead, we aim to minimize (6) iteratively using a numerical solver. For this purpose we approximate the continuous integral by a discrete sum over a frequency grid $\boldsymbol{\Omega}$ containing K samples:

$$\tilde{\mathcal{C}}(\boldsymbol{\theta}) = \frac{1}{IK} \sum_{i=1}^{I} \sum_{k=1}^{K} \Delta\Phi_{i,\log}^2(\boldsymbol{\theta}, \Omega_k) \tag{7}$$

Here, $k = 1, 2, \ldots, K$ is the frequency index and $\Omega_k \in \boldsymbol{\Omega}$. The approximation is a form of numerical integration and viable for a sufficiently dense $\boldsymbol{\Omega}$ [11]. Note that an unconstrained minimization of (7) does, in general, not lead to applicable solutions. In the following, we discuss aspects that influence the applicability of the obtained solution and show how these can be impacted by means of constraints.

A. Filter Stability Constraints

An IIR filter allows to realize unstable poles, but such a filter is not feasible. A minimization of (7) implies an inversion of the generally non-minimum-phase secondary path $S(z)$, possibly making unstable poles favorable in terms of the cost.

To prevent filter instability, the well-known all-pass expansion which mirrors unstable poles into the unit cycle could be employed [10]. Since this approach alters the design-critical phase response of the filter, we consider it to be impractical and suggest to prevent the occurrence of unstable poles through explicit constraints. We recall that an SOS cascade filter is stable if and only if all denominator coefficient pairs (a_{1l}, a_{2l}) lie within the stability triangle [12]. Since the proximity of poles to the unit circle can be problematic, e.g, due to numerical effects, we strive for a generalized condition which allows for a user defined specification of the maximum permitted pole radius $|p|_{\max}$, cf. [13]. This enables the filter's impulse response decay behavior to be controlled explicitly. We formulate a corresponding linear inequality constraint $\boldsymbol{A\theta} < \boldsymbol{b}$, where

$$\boldsymbol{A} = \left[\mathbf{0} \;\middle|\; \begin{pmatrix} -1 & -1 \\ 1 & -1 \\ 0 & 1 \end{pmatrix} \otimes \boldsymbol{I}_L \right], \qquad \boldsymbol{b} = |p|_{\max}^2 \cdot \mathbf{1}. \tag{8}$$

Here, $\mathbf{0}$ is a zero-matrix of dimension $3L \times 2L + 1$, $\mathbf{1}$ is a column vector containing $3L$ ones, $\boldsymbol{I}_L$ is the identity matrix of dimension $L \times L$ and $\otimes$ denotes the Kronecker product. The resulting filter design problem is a nonlinear optimization problem with linear inequality constraints:

$$\begin{aligned} \underset{\boldsymbol{\theta}}{\text{minimize}} \quad & \tilde{\mathcal{C}}(\boldsymbol{\theta}) \\ \text{subject to} \quad & \boldsymbol{A\theta} < \boldsymbol{b} \end{aligned} \tag{9}$$

B. Filter Magnitude Constraints

In the absence of restrictions, the magnitude response of the filter can become arbitrarily large. This might impede the applicability of the resulting filter, for example, if power specifications of the transducers are exceeded. Furthermore, a limitation for the amplification of frequency components outside the audible spectrum might be useful in cases where the filter is operated at a high sampling rate. To meet these requirements, we extend (9) by a nonlinear constraint vector $\boldsymbol{c}(\boldsymbol{\theta})$ which contains an entry

$$c(\boldsymbol{\theta}, \Omega_k) = |W(\boldsymbol{\theta}, \Omega_k)|^2 - R(\Omega_k) \tag{10}$$

for each frequency bin k. This facilitates the selective enforcement of arbitrary magnitude limits $R(\Omega) \in \mathbb{R}^{\geq 0}$. The extended optimization problem reads

$$\begin{aligned} \underset{\boldsymbol{\theta}}{\text{minimize}} \quad & \tilde{\mathcal{C}}(\boldsymbol{\theta}) \\ \text{subject to} \quad & \boldsymbol{A}\boldsymbol{\theta} < \boldsymbol{b} \\ & \boldsymbol{c}(\boldsymbol{\theta}) < \boldsymbol{0}. \end{aligned} \tag{11}$$

For the sake of completeness, we point out that regularization-based approaches can be used alternatively. These approaches involve an extension of the cost function by further terms [14], [15]. Consequently, the coefficients in the permitted range are also affected, a manual weighting of the individual terms is required and adherence to hard constraints cannot be guaranteed straightforwardly.

IV. Theoretical Upper Performance Bound

When designing $W(z)$, several effects prohibit a perfect match to the design target $H(\Omega)$ simultaneously. To study these effects in more detail, we explore a theoretical optimum that can only be achieved in the absence of constraints imposed by filter topology and order. For this we assume that $W(\Omega)$ can be chosen independently for each frequency bin, i.e.,

$$\boldsymbol{\theta} = \left(r, \varphi\right)^{\mathrm{T}}, \qquad W(\boldsymbol{\theta}, \Omega_k) = re^{j\varphi}. \tag{12}$$

In this case the global minimum of (7) can be found by solving K two-dimensional optimization problems of the form

$$\tilde{\mathcal{C}}_k(r, \varphi) = \frac{1}{I} \sum_{i=1}^{I} \Delta\Phi_{i,\log}^2(r, \varphi). \tag{13}$$

The result is a spectrum which leads to optimal performance in terms of (7) for the wearing scenario reflected by $\mathcal{I}$. The optimal spectrum is likely not realizable using a causal and stable filter with a finite number of coefficients. We note that solving (9) can be understood as an attempt to do so.

The theoretical optimum is suited to investigate the impact of transfer path variance individually. Furthermore, it provides a reference to estimate the degree of optimality for filters that strive for a minimization of (7). Performance loss resulting from an approximation of the optimal spectrum by means of a causal and stable filter can be studied separately. Since this step depends on optimization hyperparameters such as filter topology and order, it is beyond the scope of this paper.

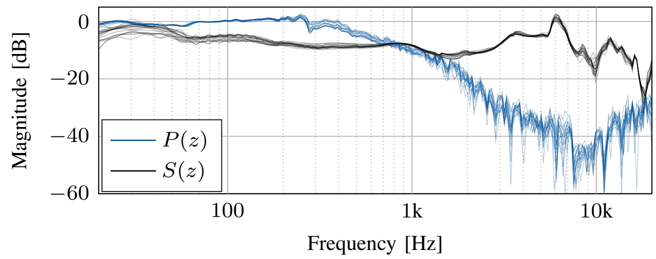

Fig. 2. Training set $\mathcal{I}$ containing $I = 20$ acoustic transfer path pairs.

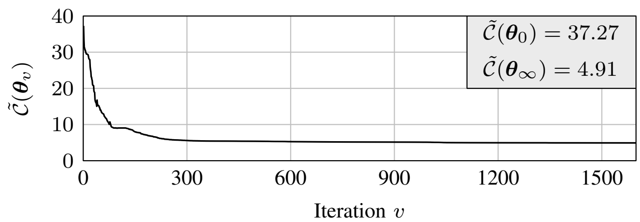

Fig. 3. Cost $\tilde{\mathcal{C}}$ over iteration v for minimization of (11) for a custom magnitude response target with two notches and one peak (cf. Fig. 4 bottom).

V. Evaluation

We conduct a two-fold evaluation of the proposed method wherein we consider simulations and real-time measurements. For this purpose, we deployed a time-invariant AAE system comprising $L = 15$ SOS on an Analog Devices ADAU1787 audio codec ($f_\mathrm{s} = 192\,\mathrm{kHz}$, $12.9\,\mu\mathrm{s}$ processing latency [16]). We used a Bose QC25 over-ear headphone without the manufacturers ANC electronics and with a direct connection to loudspeaker and microphone as an electro-acoustic front end. All measurements were conducted in a measurement room complying with the recommendation ITU-R BS.1116-2 [17] using a Head Acoustics HMS II dummy head.

For the design of the filters, a training set $\mathcal{I}$ containing $I = 20$ path pairs was measured at a sampling frequency of $f_\mathrm{s,meas} = 48\,\mathrm{kHz}$. To imitate a realistic normal fit wearing scenario, we repositioned the headphones on the dummy head after each measurement. Secondary paths were measured according to [18] using a 10 second logarithmic sweep. To measure the primary path while accounting for directional dependencies, we synthesized a diffuse pink noise sound field using 8 transducers equally distributed on the horizontal plane. Figure 2 depicts the magnitude responses of the obtained training set. For this experiment, we consider only normal fits.

A. Verification of the Average Case Performance

We evaluate the average case performance for three use-cases: maximum wideband attenuation, a flat magnitude response (hear-through) and a custom magnitude response target with two notches and one peak. We minimized (11) for these three cases using the training set, a frequency vector containing $K = 2048$ frequency samples within the audible range ($20\,\mathrm{Hz} \leq f \leq 20\,\mathrm{kHz}$) and an SQP algorithm [8]. Usually, the optimization terminates within few iterations, an example of which is shown in Figure 3.

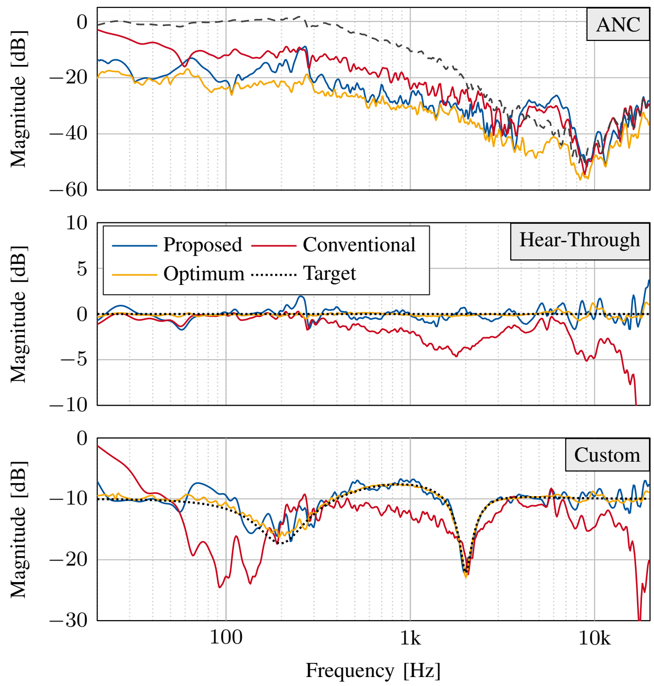

Fig. 4. Averaged transfer path magnitude response $\overline{\Phi}_{\tilde{h}\tilde{h},\log}$ for the use-cases ANC (top), hear-through (middle) and a custom target (bottom). For reference, the average passive attenuation is illustrated by a dashed line (- - - -) in the upper plot. The transfer paths (——, ——) are measurement results, whereas the optimum (——) is determined by simulation using the training set.

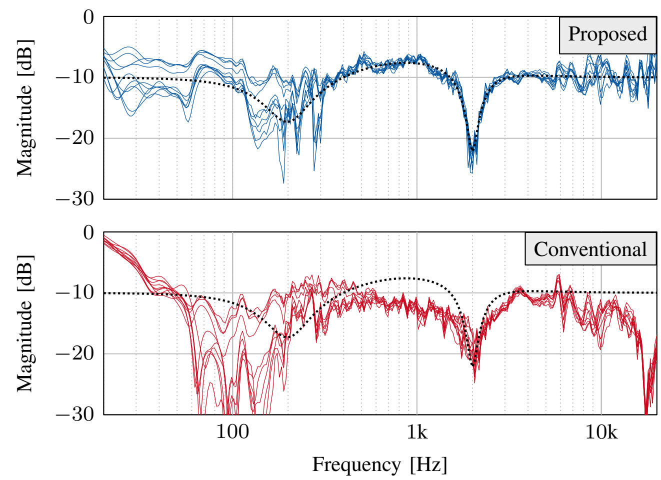

Fig. 5. Target magnitude response (⋯⋯) and measured transfer path magnitude responses $\Phi_{\tilde{h}\tilde{h},\log}$ (——/——) for the custom magnitude target. Top: proposed method, bottom: conventional method.

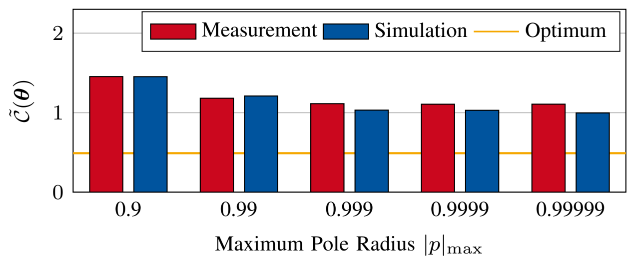

Fig. 6. Simulated and measured cost $\tilde{C}$ over maximum pole radius $|p|_{\max}$ for the hear-through use-case.

We evaluate the proposed method by measuring and subsequently averaging $I = 10$ achieved transfer paths to obtain $\overline{\Phi}_{\tilde{h}\tilde{h},\log}(\boldsymbol{\theta}, \Omega)$. We conduct the measurement as laid out in Section V for all three cases and do not consider the training set in the evaluation. We compare the proposed method to the FIR Wiener solution [3], which was converted to a SOS cascade filter ($L = 15$). Furthermore, we used the training set data to estimate a theoretical upper performance bound as discussed in Section IV.

The results of the real-time measurement are depicted in Figure 4. They verify a distinct improvement over the conventional method in terms of (7). We confirm that a simulated decrease of $\tilde{C}(\boldsymbol{\theta})$ corresponds to real-world improvements almost one-to-one. Furthermore, the proposed procedure yields filters with an objective function value that is close to the theoretical optimum. We point out that the conventional approach performs unfavorably for $f > 10\,\text{kHz}$ mainly because the generalized cost function from [3] was used to reduce the filter magnitude at high frequencies. This was necessary for the conversion to SOS with adequate accuracy.

A more detailed view is given in Figure 5, where the individual transfer path measurements that were used to obtain the averaged paths shown in the lower plot in Figure 4 are depicted. There, it can be seen that deviations from the target are also smaller for individual cases compared to the conventional approach. Furthermore, we observe that inevitable deviations caused by transfer path variance are distributed more evenly around the target compared to the conventional method.

B. Pole Radius Influence

The achievable objective function value of (9) and (11) depends on the imposed constraints. In the following, we investigate the extent to which the maximum pole radius $|p|_{\max}$ affects the achieved performance by repeating the experiment conducted in Section V-A. For this experiment, several filters with maximum pole radius $|p|_{\max}$ ranging from 0.9 to 0.99999 are designed and compared. The energy-based effective impulse response length of the filters according to [19] (99 % energy decay) ranged from 105 to 219253 samples. We restrict ourselves to the hear-through use-case and measure a second, mutually exclusive validation set containing $I = 10$ paths pairs. The resulting performance in terms of $\tilde{C}$ is compared to a simulation using the training set and depicted in Figure 6.

In terms of $\tilde{C}$, we generally observe similar performance regarding simulation and measurement. In both cases, a relaxation of the restrictions leads to better results but the benefit decreases for $|p|_{\max} \to 1$. Above $|p|_{\max} = 0.999$, all measurements indicate similar performance whereas the simulation-based performance increases slightly. This suggests the existence of a threshold above which a further increase in $|p|_{\max}$ does not lead to increased real-world performance. Possibly, the finite length of the acoustic path data contributes to this effect.

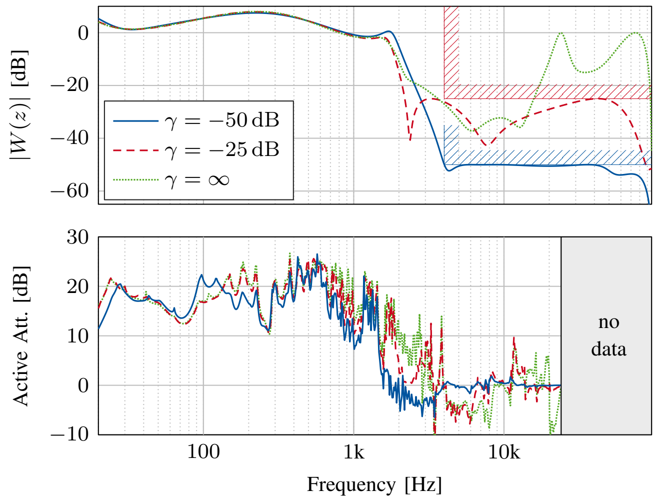

Fig. 7. Filter magnitude constraint influence for the ANC use-case: filter magnitude responses (top) and simulated average active attenuation (bottom). For $f \geq 24\,\text{kHz}$, no path data is available due to $f_{\text{s,meas}} = 48\,\text{kHz}$.

C. *Magnitude Constraint Influence*

In this section, we investigate the performance impact due to magnitude limitation as presented in Section III-B. Since the results of Sections V-A and V-B suggest a high correlation between simulated and actual performance, we investigate implications of the magnitude constraints based on a simulation using the training set. We design three filters satisfying the constraint function

$$R(\Omega) = \begin{cases} \infty, & f < 4\,\text{kHz} \\ \gamma^2, & f \geq 4\,\text{kHz} \end{cases} \tag{14}$$

for $\gamma = \{\infty, -25\,\text{dB}, -50\,\text{dB}\}$. The cut-off was set to $4\,\text{kHz}$ because in Figure 4 (top) it can be seen that the system achieves a negative active attenuation. This means that ambient noise is amplified, which is not intended.

A simulation of the resulting average active attenuation is depicted in Figure 7. In the frequency range $4\,\text{kHz}$ - $10\,\text{kHz}$, the active attenuation achieved by the filter without magnitude restriction (········) is also negative. It can be seen, however, that magnitude limitation (——) reduced this effect.

Within the remaining frequency range, the active attenuation appears to be most affected in the "transition region" ($f \approx 4\,\text{kHz}$) but is quite similar otherwise. We observe a slight performance reduction for tighter constraints, even at frequencies that are not explicitly constrained. For moderate constraints, however, this effect appears to be marginal.

VI. Conclusion

In this contribution, we formulate the feedforward ANC filter design problem for IIR filters in terms of a perceptually motivated cost function. This approach leads to a nonlinear optimization problem, upon which we impose explicit constraints in terms of stability and filter magnitude, thus providing a flexible design framework. The resulting optimization problem can be solved using iterative state of the art solvers.

We verify the performance of the presented method by means of a real time measurement for three common use cases. The measurements show a clear improvement over a state of the art approach that was used as a reference. In addition, we investigate performance implications caused by the constraints via measurement and simulation. We extend the evaluation by relating the results to a theoretical upper performance bound. The real time measurements indicate a significant step towards optimal performance.

Acknowledgment

The authors would like to thank Stefan Liebich for helpful discussions and comments on the manuscript.

References

[1] S. Liebich, J. Fabry, P. Jax, and P. Vary, "Signal processing challenges for active noise cancellation headphones," in *Speech Communication; 13th ITG-Symposium*, pp. 1–5, 2018.

[2] S. Kuo and D. Morgan, *Active Noise Control Systems: Algorithms and DSP Implementations*. Wiley, 1996.

[3] J. Fabry, F. König, S. Liebich, and P. Jax, "Acoustic equalization for headphones using a fixed feed-forward filter," in *ICASSP 2019 - 2019 IEEE International Conference on Acoustics, Speech and Signal Processing (ICASSP)*, pp. 980–984, 2019.

[4] J. Fabry and P. Jax, "Perceptual filter optimization for active acoustic equalization," in *inter-noise*, International Institute of Noise Control Engineering, 2020.

[5] J. Rämö and V. Välimäki, "An allpass hear-through headset," in *2014 22nd European Signal Processing Conference (EUSIPCO)*, pp. 1123–1127, 2014.

[6] F. Denk, H. Schepker, S. Doclo, and B. Kollmeier, "Equalization filter design for achieving acoustic transparency in a semi-open fit hearing device," in *Speech Communication; 13th ITG-Symposium*, pp. 1–5, 2018.

[7] F. Denk, *Characterizing and conserving the transmission properties of the external ear with hearing devices*. PhD thesis, 05 2020.

[8] J. Nocedal and S. J. Wright, *Numerical Optimization*. New York, NY, USA: Springer, second ed., 2006.

[9] H. Fastl and E. Zwicker, *Psychoacoustics: Facts and Models*. Springer series in information sciences, Springer Berlin Heidelberg, 2007.

[10] P. Vary and R. Martin, *Digital Speech Transmission: Enhancement, Coding and Error Concealment*. Wiley, Feb. 2006.

[11] W. Lu and A. Antoniou, "Design of digital filters and filter banks by optimization: A state of the art review," in *2000 10th European Signal Processing Conference*, pp. 1–4, 2000.

[12] L. B. Jackson, *Digital Filtering and Signal Processing with MATLAB® Exercises*. Springer, third edition ed., 1995.

[13] R. C. Nongpiur, D. J. Shpak, and A. Antoniou, "Improved design method for nearly linear-phase iir filters using constrained optimization," *IEEE Transactions on Signal Processing*, vol. 61, no. 4, pp. 895–906, 2013.

[14] O. Kirkeby and P. A. Nelson, "Digital filter design for inversion problems in sound reproduction," *J. Audio Eng. Soc*, vol. 47, no. 7/8, pp. 583–595, 1999.

[15] P. Dodds, "A flexible numerical optimization approach to the design of biquad filter cascades," *Journal of the Audio Engineering Society*, October 2020.

[16] Analog Devices. ADAU1787 Data Sheet [Online]. Accessed 05- Feb-2021.

[17] Radiocommunication Sector of International Telecommunication Union (ITU-R), *Methods for the subjective assessment of small impairments in audio systems, Recommendation ITU-R BS.1116-2*, June 2014.

[18] S. Müller and P. Massarani, "Transfer-function measurement with sweeps," *Journal of the Audio Engineering Society*, vol. 49, pp. 443–471, june 2001.

[19] T. I. Laakso and V. Valimaki, "Energy-based effective length of the impulse response of a recursive filter," *IEEE Transactions on Instrumentation and Measurement*, vol. 48, no. 1, pp. 7–17, 1999.